An archaeal biomarker record of paleoenvironmental change across the onset of the Messinian salinity crisis in the absence of evaporites (Piedmont Basin, Italy)

Marcello Natalicchio [a,*], Daniel Birgel [a,*], Jörn Peckmann [a], Francesca Lozar [b], Giorgio Carnevale [b], Xiaolei Liu [c,1], Kai-Uwe Hinrichs [c], Francesco Dela Pierre [b]

[a] Institute for Geology, Universität Hamburg, Hamburg, Germany
[b] Department of Earth Sciences, University of Torino, Torino, Italy
[c] Organic Geochemistry Group, MARUM Center for Marine Environmental Sciences and Department of Geosciences, University of Bremen, Bremen, Germany

ABSTRACT

A sudden change from normal marine to extreme paleoenvironmental conditions occurred approximately 6 Ma ago in the Mediterranean Basin at the onset of the late Miocene Messinian salinity crisis, one of the most severe ecological crises in Earth history. Strong evaporation and tectonics led to hypersaline conditions, resulting in widespread deposition of evaporites and the apparent annihilation of the marine metazoan biosphere. In contrast to the prominent occurrence of evaporites elsewhere in the Mediterranean, evaporites did not form in the deeper part of some marginal basins at the onset of the crisis. The strata of the Pollenzo section (Piedmont Basin, NW Italy) studied here were deposited in such a paleogeographic setting. Instead of evaporites, a cyclic succession of organic-rich shales and carbonates formed during the early phase of the crisis in the study area. These sediments record a sharp increase in the contents of archaeal molecular fossils that are mostly represented by isoprenoidal dialkyl glycerol diethers (DGDs) and isoprenoidal glycerol dialkyl glycerol tetraethers (GDGTs). Such an expansion of archaeal biomass is best explained by a change of the archaeal communities at the onset of the Messinian salinity crisis. In particular, the appearance of molecular fossils of extremophilic archaea, mostly producing DGDs (archaeol and extended archaeol), suggests the emergence of halophilic archaea. At the same time, lipids of planktonic Thaumarchaeota, especially crenarchaeol, are present across the entire section, suggesting the local persistence of normal marine conditions. In agreement with the sudden appearance of tetrahymanol in the upper part of the section, the persistence of crenarchaeol indicates the establishment of water column stratification after the advent of the Messinian salinity crisis. To further investigate the Piedmont Basin paleoenvironmental conditions, we test the Archaeol Caldarchaeol Ecometric (ACE), a proxy developed for identifying high paleosalinities in waters and possibly in sediments. Despite high ACE values found for the Messinian salinity crisis samples, these values are in contrast with the absence of any lithological evidence for high salinities as well with other biomarker-independent information, indicating low to normal seawater salinities. This apparent contradiction is likely explained by the complexity of the sources of archaeal lipids, especially of caldarchaeol and archaeol, limiting the utility of the ACE for the reconstruction of paleosalinities for Messinian strata.

1. Introduction

Isoprenoidal glycerol dialkyl glycerol tetraethers (GDGTs) and isoprenoidal dialkyl glycerol diethers (DGDs) are the two most common types of membrane lipids of Archaea. Among the Thaumarchaeota and Crenarchaeota, GDGTs are the predominating membrane lipids (Schouten et al., 2013; Elling et al., 2017). Among the Euryarchaeota, GDGTs are less abundant than DGDs (Koga et al., 1998), or even absent as in halophilic archaea (e.g.,

* Corresponding authors.
  E-mail addresses: marcello.natalicchio@uni-hamburg.de (M. Natalicchio), daniel.birgel@uni-hamburg.de (D. Birgel).
[1] Address: Department of Earth, Atmospheric, and Planetary Sciences, Massachusetts Institute of Technology, 77 Massachusetts Avenue, Cambridge, MA 02139-4307, USA.

Dawson et al., 2012); only the uncultured anaerobic methane oxidizing archaea are known to produce as well high amounts of GDGTs (e.g., Blumenberg et al., 2004). The stable isoprenoid-containing and ether-bond membrane lipids of Archaea are believed to be advantageous for adaptation to harsh environmental conditions (e.g., De Rosa and Gambacorta, 1988; Schouten et al., 2013 and References therein), including high temperatures, salinities, and concentrations of reduced chemical compounds such as hydrogen sulfide. Likewise, archaeal molecular fossils, and especially DGDs and their degradation products, have commonly been used for the reconstruction of ancient extreme environments such as methane seeps (e.g., Schouten et al., 2003, 2007, 2013; Blumenberg et al., 2007; Birgel et al., 2008) and hypersaline basins (Teixidor et al., 1993; Grice et al., 1998; Turich and Freeman, 2011; Birgel et al., 2014, 2015; Christeleit et al., 2015).

A prominent example of an ancient hypersaline basin is the late Miocene Mediterranean Basin, which experienced a sudden change from normal marine to extreme hypersaline conditions during the Messinian salinity crisis (MSC) about 6 Ma ago (Hsü et al., 1977; Krijgsman et al., 1999; Ryan, 2009; Roveri et al., 2014). The progressive isolation of the Mediterranean Sea from the Atlantic Ocean, triggered by the tectonic closure of the Betic and Rifian gateways, caused the transformation of the Mediterranean Sea into a giant salina (Flecker et al., 2015; Capella et al., 2016). The Mediterranean waters became increasingly salty, leading to the deposition of more than 1 million km^3 of evaporites (carbonate minerals, gypsum, halite) on the Mediterranean seafloor in less than 700 ka (e.g., Roveri et al., 2014). The lack of modern analogs for such a basin-wide evaporite event hampers a reliable environmental reconstruction and makes this paleoenvironmental crisis one of the most controversial events of Earth history (Roveri et al., 2014).

In Messinian peripheral basins, the occurrence of gypsum is the most striking evidence of increasing salinity; this lithological marker is consequently commonly used to trace the onset of the MSC. However, gypsum was typically only deposited in the most marginal sectors of these peripheral basins, which experience a downslope transition into shales and carbonate-rich deposits lacking evaporites (Manzi et al., 2007, 2016; Gennari et al., 2013, in press). The timing of the MSC is now well constrained (e.g., Roveri et al., 2014), but the physico-chemical conditions that became established during the MSC and their impact on the marine ecosystem are still poorly understood. The change in seawater chemistry apparently caused the overall demise of eukaryotes, particularly metazoans (e.g., Bellanca et al., 2001). In contrast to the majority of eukaryotes, prokaryotes and especially the versatile archaeal domain are believed to be more tolerant of extreme environmental conditions, and molecular fossils of archaea may consequently serve to trace the environmental changes in the course of the MSC (e.g., Turich and Freeman, 2011; Christeleit et al., 2015).

Here, we investigate the molecular fossil inventory of the Pollenzo section (Fig. 1; Piedmont Basin, NW Italy) with its cyclic succession of marls, shales, and carbonate-rich beds, focusing on archaeal lipids. Molecular fossils of archaea are well preserved and abundant throughout the studied section and prove to be excellent recorders of changing environmental conditions across the MSC onset in the absence of evaporite deposition.

2. Geological setting

The study area is located in the Piedmont Basin (NW Italy), a wedge-top basin filled with Upper Eocene to Messinian deposits (Fig. 1B; Maino et al., 2013). The Messinian strata are exposed both in its northern and southern margins (Fig. 1C; Dela Pierre et al., 2011). At the southern margin (Langhe region), where the studied Pollenzo section is located, the Messinian succession starts with outer shelf to slope muddy sediments referred to as the Sant'Agata
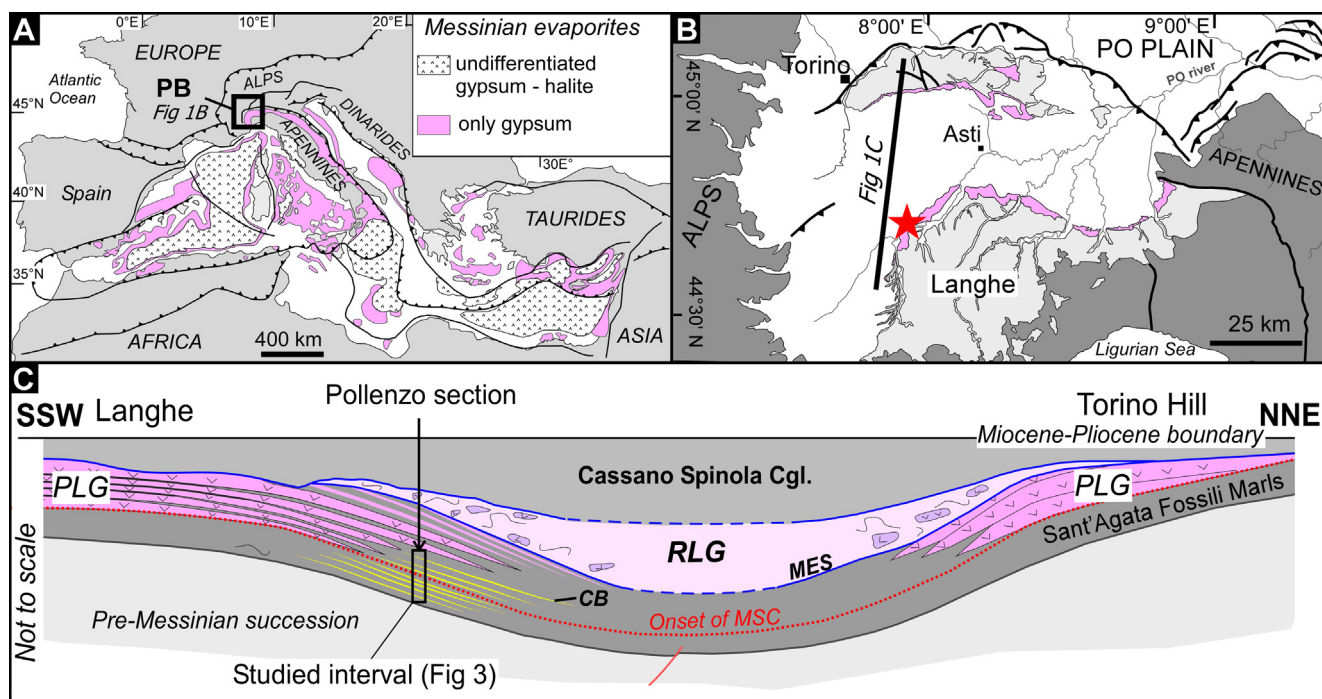

Fig. 1. (A) Distribution of the Messinian evaporites in the Mediterranean Basin (modified from Manzi et al., 2012; PB: Piedmont Basin). (B) Geological sketch of the Piedmont Basin (box in Fig. 1A) showing the areal distribution of Messinian deposits (in pink) (modified from Dela Pierre et al., 2011); the red star indicates the Pollenzo section (44°41'08″N; 7°55'33″E). (C) Simplified profile (NNE–SSW direction, see Fig. 1B) showing the distribution of the Messinian deposits across the western Piedmont Basin (modified from Dela Pierre et al., 2011). The location of the Pollenzo section is indicated. PLG: Primary Lower Gypsum unit; RLG: Resedimented Lower Gypsum unit; MES: Messinian Erosional Surface; CB: carbonate-rich beds. (For interpretation of the references to colour in this figure legend, the reader is referred to the web version of this article.)

Fossili Marls (Tortonian–lower Messinian), recording progressively more restricted conditions heralding the onset of the MSC. This unit displays a marked lithological cyclicity (Fig. 2A), evidenced by the rhythmic repetition of shale/marl couplets (Lozar et al., 2010; Dela Pierre et al., 2011; Violanti et al., 2013). Such cyclicity is assumed to reflect precession-driven climate change with a periodicity of about 20 ka (Krijgsman et al., 1999; Manzi et al., 2012).

At the basin margins, the Sant'Agata Fossili Marls are overlain by primary sulfate evaporites referred to as the Primary Lower Gypsum unit (sensu Roveri et al., 2008; Fig. 1C). This gypsum was deposited during the first MSC stage (5.97–5.60 Ma), and also shows precession-driven lithological cyclicity, represented by shale/gypsum couplets (Dela Pierre et al., 2011). Very low salinity recorded by gypsum fluid inclusions (average of 1.6% NaCl equivalent), which is lower than sea water salinity, points to a strong contribution from freshwater in the Piedmont Basin during the deposition of the Primary Lower Gypsum (Natalicchio et al., 2014). Interestingly, the isotope signatures of the sediments of the Pollenzo section deposited after the MSC onset are marked by a sharp decline of $\delta^{18}O$ values ($\delta^{18}O$ as low as $-9\permil$ V-PDB; Dela Pierre et al., 2012), agreeing with strong freshwater influx during the early phases of the MSC.

Towards the basin depocenter, gypsum makes a transition into a cyclic succession of shales, marls, and carbonate-rich beds belonging to the Sant'Agata Fossili Marls. In particular, seven lithological cycles (Pm1–Pm7) with an average thickness of 3 m have been recognized (Fig. 2A), which were deposited at water depths of more than 200 m, according to benthic foraminifer assemblages from the lower four cycles (Pm1–Pm4; Violanti et al., 2013). Each cycle is composed of a basal layer of laminated shale that passes into a marly horizon and a dm-thick carbonate-rich bed. This cyclical pattern has been tuned to orbital solution (Laskar et al., 2004) using biostratigraphic tie points and correlated bed by bed to the Abad (Perales) reference section (Sierro et al., 2001). In the Pollenzo section, the onset of the MSC has been identified at the base of cycle Pm5, three precessional cycles below the first gypsum bed;

the latter was deposited approximately 60 ka after the MSC onset (Lozar et al., 2010, in press). In detail, the upper part of the Sant'Agata Fossili Marls comprises four pre-MSC cycles (Pm1–Pm4) and three MSC cycles (Pm5–Pm7), which are the deeper water counterparts of the lower three Primary Lower Gypsum cycles in the marginal part of the basin (Figs. 1C and 2A). Average sedimentation rates are thought to be constant across the MSC onset, corresponding to approximately 15 cm/ka. MSC deposits, both carbonate-rich beds (beds e, f and g) and unconsolidated layers, are well laminated (Fig. 2B and C) and are typified by a mass occurrence of filaments (Fig. 2D), interpreted to represent fossils of colorless sulfide-oxidizing bacteria (Dela Pierre et al., 2012) that apparently correspond to filamentous fossils in Messinian gypsum deposits (Dela Pierre et al., 2015).

3. Materials and methods

3.1. Sample preparation

Two freshly exposed lithological pre-MSC cycles (Pm3 and Pm4) and three MSC cycles (Pm5, Pm6 and Pm7; Fig. 2A) of the Pollenzo section were studied. Forty-four samples were analyzed for total organic carbon (TOC) and 15 samples for molecular fossil contents (see Fig. 3 for sample positions). Among them, five samples are from the carbonate-rich layers (beds c to g; Fig. 3) and 10 samples from the unconsolidated sediments. Since the lipid biomarker patterns observed remained unchanged in both lithologies, equal preservational conditions are expected.

3.2. Total organic carbon

For TOC contents, samples were taken at high resolution in order to trace the trends across the MSC onset. The sediments were dried and ground with a mortar and pestle. After splitting the samples into two aliquots, the total carbon (TC) content was deter-
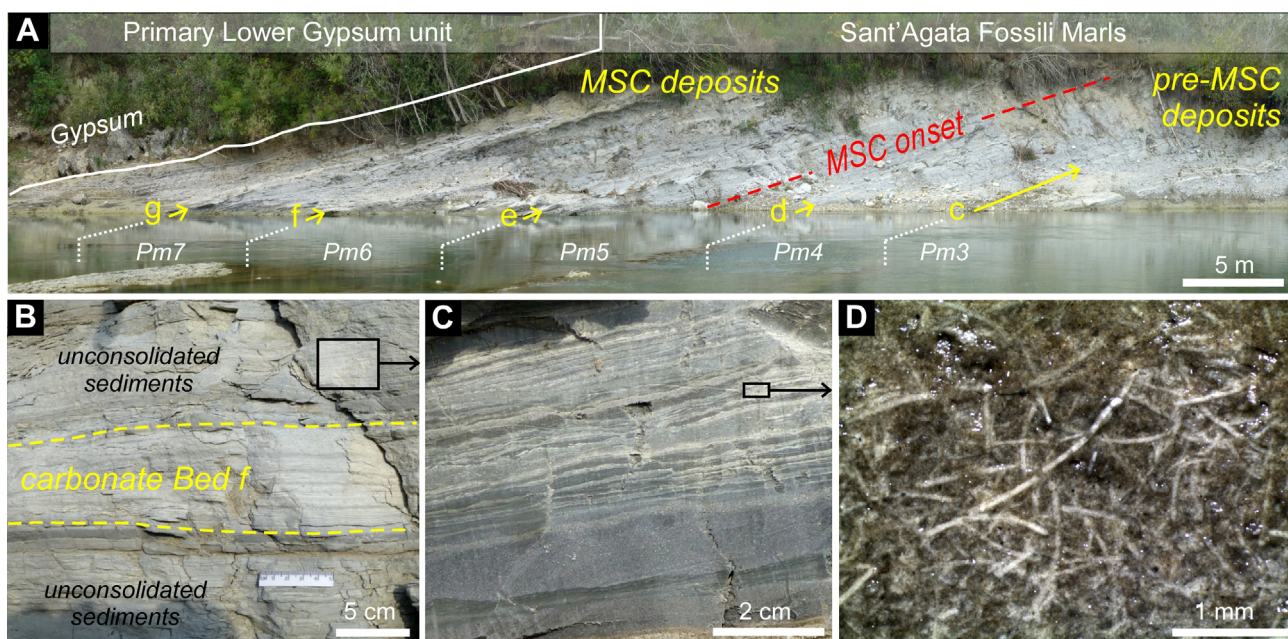

Fig. 2. (A) Outcrop view of the Pollenzo section archiving the onset of the Messinian salinity crisis (MSC); the letters in yellow refer to the carbonate layers. Lithological cycles (Pm3–Pm7) are indicated by dashed white lines. (B and C) Close-up views of a horizon with laminated carbonate layers (B) and the unconsolidated sediments above it (C); the latter revealed high yields of archaeal lipids. (D) Layer surface with fossilized filaments interpreted to represent sulfide-oxidizing bacteria (Dela Pierre et al., 2012). The boxes in (B) and (C) indicate the details shown in Figs. (C) and (D), respectively. (For interpretation of the references to colour in this figure legend, the reader is referred to the web version of this article.)
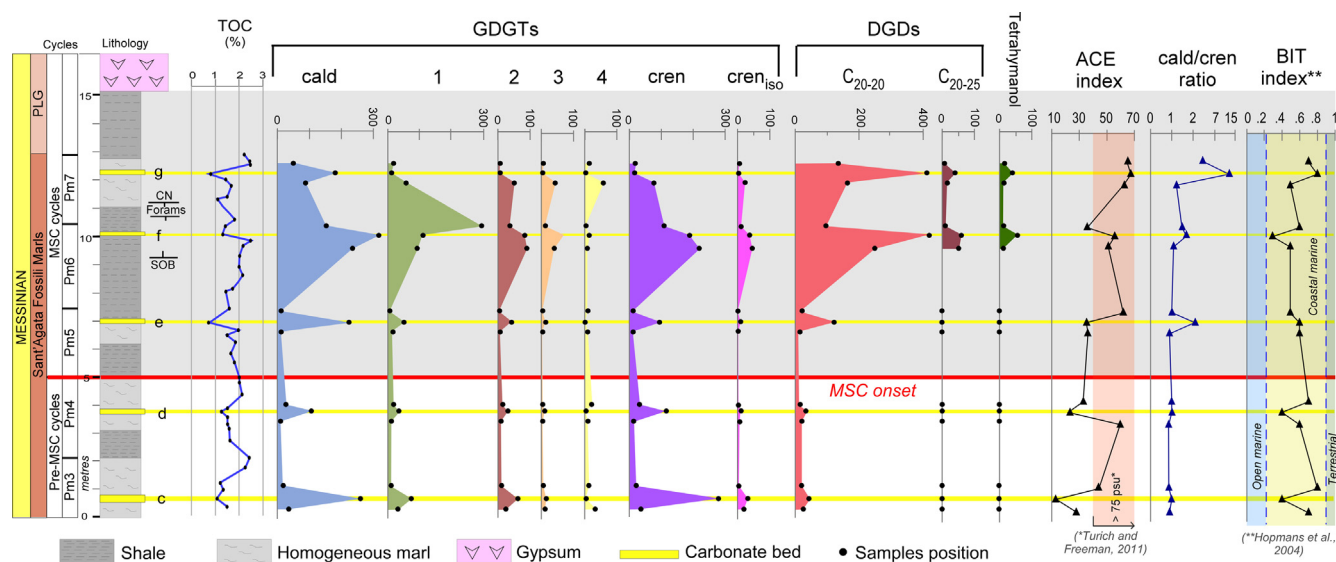
Fig. 3. Graphs showing the contents of total organic carbon (TOC; %), major archaeal compounds (GDGT$_{0-4}$, crenarchaeol, DGDs), and tetrahymanol (μg/g TOC). On the right, the Archaeol and Caldarchaeol Ecometric (ACE) index, the caldarchaeol/crenarchaeol ratio, and the BIT index are shown. The gray shaded area represents the deposits of the Messinian salinity crisis. The first occurrence of filaments of putative sulfide-oxidizing bacteria (SOB) and the last occurrences of calcareous nannofossils (CN) and foraminifers are indicated. C$_{20-20}$:C$_{20-20}$ archaeol; C$_{20-25}$:C$_{20-25}$ archaeol; GDGTs: glycerol dialkyl glycerol tetraethers; DGDs: diphytanyl glycerol diethers; cald: caldarchaeol; cren: crenarchaeol; cren$_{iso}$: crenarchaeol regio isomer; PLG: Primary Lower Gypsum unit.

mined with a LECO SC-144DR Carbon Analyzer equipped with an infrared detector at 1350 °C at the Institute for Geology of the University of Hamburg. The second aliquot was heated first to 550 °C for 5 h to remove organic carbon and then heated to 1350 °C to measure the carbon content (IC); TOC contents were determined by the formula TOC = TC − IC. A Synthetic Carbon Leco 502-029 (1.01 ± 0.02 carbon%) standard was measured prior to and after sample analyses.

3.3. Molecular fossil analyses

Carbonate samples were decalcified with 10% HCl until ~75% of the carbonate was dissolved. The detailed cleaning, decalcification, and extraction procedure applied in this study has been published elsewhere (Birgel et al., 2006). The dry non-carbonate sediments were homogenized with a mortar and pestle. The remaining residual sediment after decalcification and the unconsolidated sediments were first saponified with 6% KOH in MeOH using an ultrasonic bath to release matrix-bound carboxylic acids (2 h at 80 °C). The saponification extract was collected in a separatory funnel. Then, all samples were extracted by ultrasonication with dichloromethane (DCM):MeOH (3:1, v:v) and repeated until the extracts became colorless. The combined extracts were treated with 10% HCl to pH 1 to transfer the free fatty acids to the organic solvent phase. For gas chromatography (GC) analysis, each extract was pre-cleaned by separation into *n*-hexane-soluble and dichloromethane-soluble fractions. The *n*-hexane fraction was further treated and separated via solid phase extraction using a Supelco glass cartridge (6 ml, 500 mg, DSC-NH$_2$) into four fractions of increasing polarity: (a) hydrocarbons with 4 ml *n*-hexane, (b) ketones with 6 ml *n*-hexane:DCM (3:1, v:v), (c) alcohols with 7 ml DCM:acetone (9:1, v:v), (d) carboxylic acids with 8 ml 2% formic acid in DCM. Alcohols were derivatized by adding 100 μl pyridine and 100 μl N,O-*bis*(trimethylsilyl)trifluoroacetamide (BSTFA) to the alcohol fraction at 70 °C for 30 min. The derivatized fraction was dried under a stream of N$_2$ and re-dissolved in *n*-hexane prior injection. Free carboxylic acids were reacted with 1 ml 14% BF$_3$ in MeOH at 70 °C for 1 h to form fatty acid methyl esters. After cooling, the mixture was extracted four times with 2 ml *n*-hexane.

Combined extracts were evaporated under a stream of N$_2$, and re-dissolved in *n*-hexane prior to injection. The hydrocarbon fraction, the derivatized alcohol, and carboxylic acid fractions were analyzed using coupled gas chromatography–mass spectrometry (GC–MS) with an Agilent 7890 A GC system coupled to an Agilent 5975C inert MSD mass spectrometer at the Department of Geodynamics and Sedimentology, University of Vienna. Quantification was done using GC-flame ionization detection (GC-FID) with an Agilent 7820 A GC system. Internal standards used were 5α-cholestane for hydrocarbons, 1-nonadecanol for the alcohols, and 2-Me-C$_{18}$ fatty acid for the carboxylic acids. Both GC systems were equipped with a HP-5 MS UI fused silica column (30 m × 0.25 mm i.d., 0.25 μm film thickness). The carrier gas was helium. The GC temperature program for all fractions was: 60 °C (1 min); from 60 °C to 150 °C at 10 °C/min; from 150 °C to 320 °C (held 25 min) at 4 °C/min. Compound assignment was based on retention times and published mass spectral data.

3.4. GDGT and DGD analysis

For examination of glycerol dialkyl glycerol tetraethers (GDGTs; Fig. 4) an aliquot of the solvent extract, that was dissolved in *n*-hexane/isopropanol (99.5:0.5, v:v), was analyzed following the recently developed tandem column protocol (Becker et al., 2013). GDGT distributions were measured with a Bruker Maxis Accurate-Mass Quadrupole Time-of-Flight (qToF) mass spectrometer connected to a Dionex Ultimate 3000 RS ultra high performance liquid chromatography (UHPLC) system via an atmospheric pressure chemical ionization (APCI) interface. Separation of GDGTs was done with ACQUITY UPLC ®BEH Hilic Amide columns (2.1 × 150 mm, 1.7 μm, Waters) maintained at 50 °C. The solvent gradient program was: constant 0.5 ml/min and a linear gradient from 3% B to 20% B in 20 min, then increased linearly to 50% B at 35 min, after which to 100% B at 45 min, held 6 min, finally back to 3% B for 9 min for re-equilibration of the column; solvent A was *n*-hexane and B *n*-hexane/isopropanol (90:10, v:v). Detection of GDGTs was achieved by using positive ion APCI. The APCI source parameters were: corona current 3500 nA, nebulizer gas 5 bar, drying gas 8 l/min, drying gas 160 °C, vaporizer 400 °C. The scan range
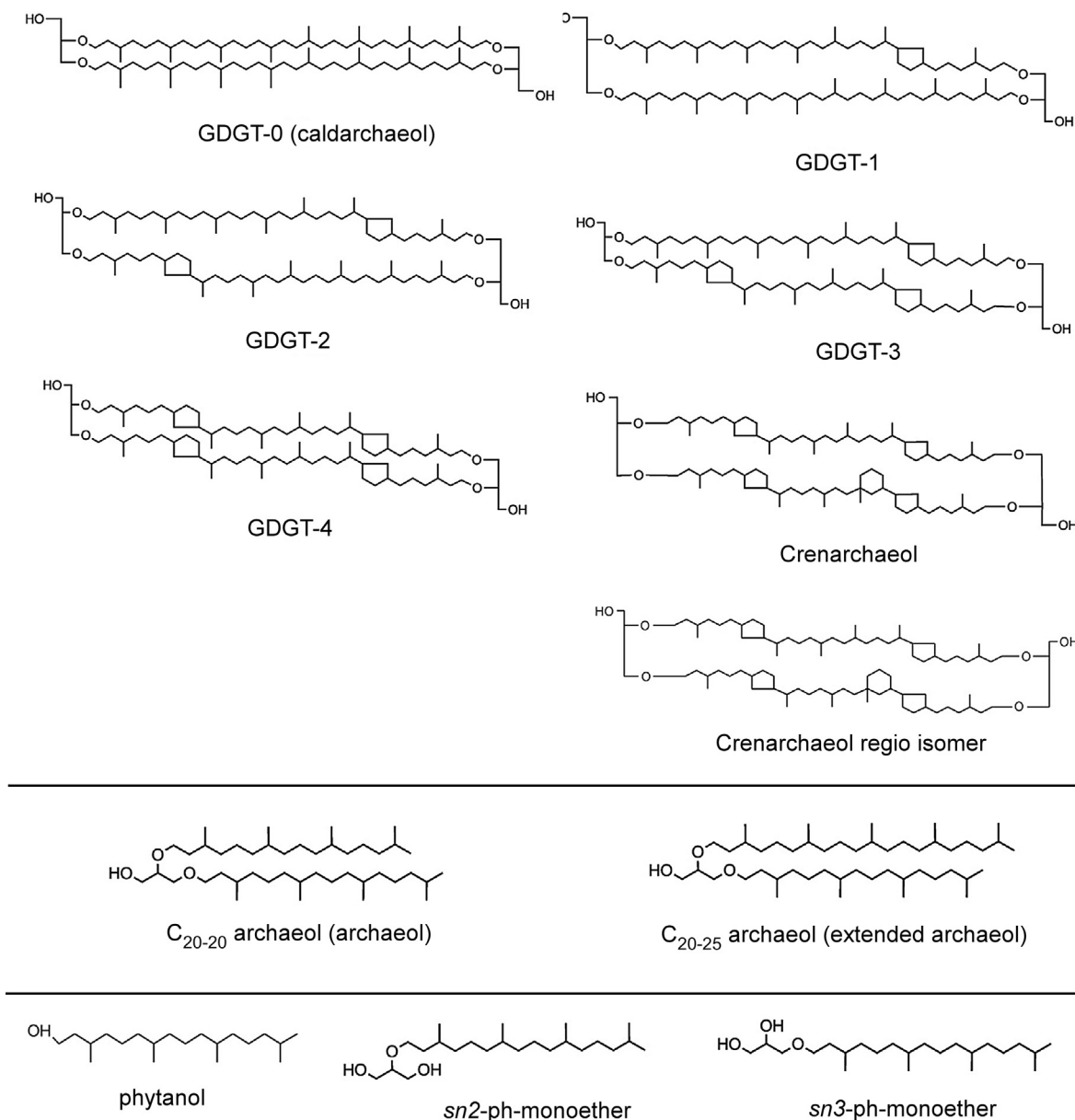
Fig. 4. Structures of archaeal isoprenoid alcohols in the Pollenzo samples.

was m/z 150–2000 at a rate of 2 Hz. GDGTs were assigned from accurate mass (better than 1 ppm), retention time, and diagnostic fragments (Liu et al., 2012). No internal standard was added for the quantification of GDGTs. Quantification was carried out indirectly by correlating GC–MS and HPLC–APCI-MS data for each sample, using GC- and HPLC-amenable archaeol as reference. Archaeol was quantified using GC-FID with an internal standard in the alcohol fraction (1-nonadecanol). To verify the relative response factors of archaeol and GDGT-0 for the applied HPLC–APCI-MS settings, a standard mix solution containing 10 ng of archaeol and GDGT-0 was injected into the system at various concentrations (see Supplementary material for more information). The response factors of archaeol and GDGT-0 are 1.07 and 1, respectively in our samples and not 30 for archaeol, as shown by Turich and Freeman (2011). In some studies, the response factor was only indirectly determined; for instance, Christeleit et al. (2015) compared measured salinities of a known reference sample with the results achieved by measuring archaeol and GDGT-0. The same is true for the study of Wang et al. (2013), where no response factor calculation was

made. The very significant variations of the response factors between previous studies and our results, especially those relevant for the Archaeol and Caldarchaeol Ecometric (ACE; e.g., Turich and Freeman, 2011; Wang et al., 2013; Christeleit et al., 2015), may have a substantial influence on the determination of the quantities of archaeol and caldarchaeol and the calculation of the ACE itself.

3.5. GDGT and DGD indices

The branched isoprenoid tetraether (BIT) index was calculated accordingly to the equation [Eq. 1] after Hopmans et al., 2004:

$$BIT = (I + II + III)/(I + II + III + crenarchaeol) \qquad (1)$$

where I, II and III refer to the branched GDGTs with m/z 1022, 1036 and 1050 respectively (refer to Hopmans et al., 2004 for the molecular structures of the branched GDGTs). This index is based on the relative abundance of terrigenous branched non-isoprenoidal tetraethers versus the marine-derived crenarchaeol and is used to iden-

tify the contribution of land-derived organic matter (cf. Hopmans et al., 2004).

The ACE (Turich and Freeman, 2011) was calculated for estimating the magnitude of the salinity change at the onset of the MSC according to the equation [Eq. 2] provided by Turich and Freeman (2011):

$$ACE = [archaeol/(archaeol + caldarchaeol)] \times 100 \qquad (2)$$

This index, based on the relative abundance of these two isoprenoids, is believed to reflect changes in the archaeal community structure in response to salinity changes (Turich and Freeman, 2011; Wang et al., 2013).

Salinities were calculated from the ACE index using the equation [Eq. 3] of Turich and Freeman (2011):

$$Salinity = (ACE + 9.7)/0.38 \qquad (3)$$

using a calibration ($R^2 = 0.95$) that excludes significant input of terrestrial material.

4. Results

4.1. Total organic carbon contents

TOC contents vary from 0.7% to 2.5% and show a periodical oscillation both in the pre-MSC and MSC lithological cycles (Fig. 3 and Supplementary Table S1); the lowest TOC contents were found in the carbonate-rich beds and, in particular, in beds e and g (TOC = 0.7%), whereas higher contents were measured in the laminated shales of cycles Pm3, Pm6, and Pm7 (approximately 2.5%).

4.2. Lipid biomarker inventory

4.2.1. Isoprenoid alcohol distribution

In the Pollenzo section, isoprenoid alcohols are the most abundant compounds, representing on average 35 wt% and 31 wt% of the total extractable lipid content in the pre-MSC and MSC deposits, respectively (Table 1; see Supplementary Table S2 for complete isoprenoid alcohol data). Isoprenoid alcohols are predominated by DGDs and GDGTs (Table 2, Figs. 3 and 4, Supplementary Table S2) and their contents increase more than two times above the MSC onset, from a total average abundance of 267 µg/g TOC in the

pre-MSC deposits to 633 µg/g TOC in the MSC ones (Table 1). In particular, the rise in DGD and GDGT abundances occurs just below Bed f (Fig. 3), approximatively one precessional cycle above the MSC onset.

Interestingly, the distribution of the major GDGTs changes across the MSC onset (Table 2). GDGTs are the dominant group in pre-MSC sediments, making up 92% of all isoprenoid alcohols. The two major GDGTs, GDGT-0 (caldarchaeol) and crenarchaeol are evenly distributed across the pre-MSC deposits (caldarchaeol/crenarchaeol ratio ∼1) and represent half of the archaeal isoprenoid alcohols identified. They are accompanied by GDGTs with 1–4 cyclopentane rings (Table 2). Among the latter, GDGT-1 and GDGT-2 are more abundant, whereas GDGT-3 and GDGT-4 make up the least of all GDGTs. Above the MSC onset, the relative average proportions of caldarchaeol (21%) and crenarchaeol (12%) have changed (Table 2), with a consequent increase of the caldarchaeol/crenarchaeol ratio up section from a value of ∼1 at the MSC onset to a value of 13 in Bed g. Maximum caldarchaeol and crenarchaeol contents were found in carbonate Bed f and in the

Table 2
Average content and percentage of isoprenoid alcohols in the Messinian deposits (% of total isoprenoid alcohols) and total amount of the diphytanyl glycerol diethers (DGDs) and glycerol dialkyl glycerol tetraethers (GDGTs).

Compound	Average amount			
	Pre-MSC (n = 6)		MSC (n = 9)	
	(µg/g TOC)	(%)	(µg/g TOC)	(%)
C_{20}–C_{20} archaeol	22	7.2	182	25.8
C_{20}–C_{25} archaeol	0	0.0	20	2.8
Total DGDs	*22*	*7.2*	*202*	*28.5*
GDGT-0 (caldarchaeol)	77	24.9	147	20.8
GDGT-1	30	9.8	74	10.4
GDGT-2	26	8.5	36	5.1
GDGT-3	7	2.4	21	2.9
GDGT-4	14	4.6	13	1.8
Crenarchaeol	83	27.0	84	11.9
Crenarchaeol isomer	47	15.2	83	11.7
Total GDGTs	*285*	*92.4*	*458*	*64.7*
Phytanol	1	0.3	31	4.3
*sn*2-ph-monoether	0	0.0	14	1.9
*sn*3-ph-monoether	0	0.0	4	0.5
Sum (µg/g TOC)	309		707	

Table 1
Molecular fossils inventory with average content and percentage (% of the total extractable lipid content) of the studied Messinian deposits.

Compounds	Source	Average amount			
		Pre-MSC (n = 6)		MSC (n = 9)	
		(µg/g TOC)	(%)	(µg/g TOC)	(%)
Isoprenoid alcohols[*]	Archaea	267	34.8	633	31.4
Branched GDGTs[**]	Bacteria	59	7.7	103	5.1
n-C_{16} and *n*-C_{18}-FA	Algae, Bacteria	74	9.7	108	5.3
Branched FA[***]	Bacteria	70	9.1	43	2.1
McDGs	Bacteria	3	0.4	6	0.3
Hopanoids[****]	Bacteria	15	1.9	115	5.3
Tetrahymanol	Ciliates, Bacteria	0	0	15	0.7
Sterols[§]	Algae, land plants	47	6.2	234	10.3
LC *n*-fatty acids	Land plants (algae)	43	5.6	230	11.4
MC *n*-fatty acids	Algae, zooplankton	28	3.7	96	4.7
LC *n*-alcohols	Land plants	68	8.9	234	11.6
LC *n*-alkanes	Land plants	92	12.0	236	11.7
Sum (µg/g TOC)		766		2020	

LC: long chain (with 25–33 carbons); MC: medium chain (with 20–24 carbons); FA: fatty acids; McDG: macrocyclic diether lipids.
[*] GDGTs; DGDs; *sn*2-ph-monoether; *sn*3-ph-monoether; phytanol.
[**] see supplementary material for more details (Supplementary Table S3).
[***] *i*, *ai*-C_{15}; C_{16}, C_{17}, 10Me-C_{16}.
[****] C_{32} ββ–hopanol, C_{31} ββ–hopanoic acid, C_{32} ββ–hopanoic acid, 2Me C_{32} ββ–hopanoic acid, 3Me C_{32} ββ–hopanoic acid.
[§] Sitosterol, dinosterol.

shales just below, with 327 and 239 µg/g TOC for caldarchaeol, and 189 and 222 µg/g TOC for crenarchaeol, respectively (Fig. 3 and Supplementary Table S2). Overall, the other GDGTs (1–4) also increase in cycles Pm6 and Pm7 (especially in and close to Bed f), but decline in the uppermost part of cycle Pm7 (Bed g; see Fig. 3).

Changes in DGD distributions between pre-MSC and MSC deposits are even more significant. In the pre-MSC section, DGDs are represented only by C_{20-20} archaeol (Fig. 3), which accounts for about 7% of all isoprenoid alcohols on average (Table 2). On the contrary, in the MSC sediments, C_{20-20} archaeol increases significantly and is more than four times more abundant than in the pre-MSC sediments on average. C_{20-20} archaeol peaks in carbonate layers f (396 µg/g TOC) and g (384 µg/g TOC) (Supplementary Table S2). This extreme increase of C_{20-20} archaeol contents (26% of all isoprenoid alcohols in the upper part of the section) is accompanied by the first appearance of a second DGD, C_{20-25} archaeol (extended archaeol). Extended archaeol represents 3% of all the isoprenoid alcohols (Table 2) and it shows the maximum abundances in Bed f and in the shales just below (~58 µg/g TOC) (Fig. 3 and Supplementary Table S2).

Apart from GDGTs and DGDs, also minor amounts of phytanol and *sn*2- and *sn*3-phytanyl-monoethers have been identified. The phytanol contents are 87 and 113 µg/g TOC in Beds f and g, respectively (Supplementary Table S2). This compound is present only in very minor amounts in the pre-MSC deposits. The two phytanyl-monoethers (*sn*2 and *sn*3) appear coevally with extended archaeol. Their maximum abundances mirror that of the other archaeal ether lipids with a total of 52 µg/g TOC in Bed f and of 68 µg/g TOC in Bed g.

4.2.2. Distribution of other lipids

Other groups of compounds that have been identified (data not shown in detail; see Table 1 for the relative abundances) include sterols, long chain *n*-alcohols (C_{26}–C_{32}), long chain *n*-alkanes (C_{26}–C_{31}), long chain *n*-fatty acids (C_{26}–C_{32}), and various hopanoids. As found for the isoprenoid alcohols, most compound contents significantly increase from the pre-MSC to the MSC deposits; hopanoids increase from 15 to 115 µg/g TOC, sterols from 47 to 234 µg/g TOC, and long chain *n*-fatty acids from 43 to 230 µg/g TOC on average, respectively. Some compounds, like the pentacyclic triterpenoid tetrahymanol was identified only in the MSC deposits, with slightly higher contents in carbonate beds (up to 52 µg/g TOC in Bed f; see Table 1, Fig. 3 and Supplementary Table S2). Other compounds do not increase as significantly as the aforementioned compound classes, as for example branched GDGTs (Supplementary Table S3 shows the abundance of the compounds used to calculate the BIT index; Hopmans et al., 2004, see below), n-C_{16} and n-C_{18}, and other, medium chain fatty acids. Various branched fatty acids even decrease after the onset of the MSC. Two non-isoprenoidal macrocyclic diether lipids (McDGs: B and C in Baudrand et al., 2010) were found with very low abundances in the pre-MSC and MSC sediments.

4.2.3. GDGT and DGD-based indices

The obtained BIT values range from 0.3 to 0.8 (see Supplementary Table S3; Fig. 3). The lowest values (0.3–0.4) are recorded in carbonate Beds c, d and f, coinciding with an increase of the crenarchaeol contents. Highest BIT values (0.7–0.8) are observed in the shales from the lowermost part of the section (cycles Pm3 and Pm4), as well as in carbonate Bed g.

Concerning the ACE index and calculated salinities (Fig. 3 and Supplementary Table S2), the values in the carbonate layers increase up section, from an ACE value of 14 in Bed c to a value of 67 in Bed g, with calculated salinities increasing from 61 ppt to 201 ppt. Shale layers show a less distinctive trend and exhibit greater fluctuations, with minimum ACE and salinities values below Bed c (~28 and ~99 ppt; respectively) and maximum values above Bed g (~64 and ~195 ppt, respectively). Remarkably, values as high as 59 were found also in the pre-MSC deposits; according to the Eq. 3 (Turich and Freeman, 2011), such values corresponds to a salinity of 180 pppt.

5. Discussion

5.1. Archaeal expansion and diversification across the onset of the Messinian salinity crisis

In the Pollenzo section, the predominance of isoprenoid alcohols, but especially of DGDs and GDGTs, indicates that archaea were among the most abundant organisms before and after the onset of the crisis (Table 1). Right after the advent of the MSC, archaeal lipids begin to increase significantly at constant sedimentation rates (Fig. 3). The general increase of isoprenoid alcohols is accompanied by a rise of other, non-isoprenoidal molecular fossils (Table 1). In particular, the concomitant increase of long-chain aliphatic compounds (see Table 1), which derive from leaf waxes of terrestrial higher plants (e.g., Eglinton and Hamilton, 1967), suggests that the increased contents of archaeal lipids may reflect an enhanced supply of terrestrial organic matter, and consequently an input of biomass from soil archaea (e.g., Pester et al., 2011). However, the BIT values do not reveal a trend of increasing input of soil-derived organic matter in the Pollenzo section and are chiefly in the range of coastal marine environments (Hopmans et al., 2004). Such BIT values (0.3–0.5) suggest that input from soil archaea did not affect the overall archaeal lipid inventory and confirm that aquatic archaea contributed significantly to marine biomass production in the water column; part of this biomass was subsequently exported to the seafloor and preserved in the sediments.

Apart from the unusually high contents of archaeal lipids in the MSC deposits, there are no changes in the relative proportion of isoprenoid alcohols compared to other compounds, since contents of most non-isoprenoidal molecular fossils increase as well (Table 1). Nevertheless, it must be noted that a relevant change in the composition of the archaeal isoprenoid alcohol inventory occurred after the MSC onset, exemplified by an extreme rise of C_{20-20} archaeol and the first appearance of C_{20-25} archaeol (extended archaeol) just below Bed f. The DGD and GDGT patterns of the Pollenzo MSC deposits resemble patterns found in extreme environments, such as methane seeps (e.g., Pancost and Sinninghe Damsté, 2003; Birgel et al., 2008) and hypersaline environments (Turich and Freeman, 2011). However, the isoprenoid alcohol patterns also show some differences from those of methane seep environments (e.g., Blumenberg et al., 2004), with their prominent GDGTs 1–3 (which are present only in low amount in the MSC sediments) and the absence of crenarchaeol. Hypersaline environments, on the other hand, are typified by a predominance of C_{20-20} archaeol and C_{20-25} archaeol (extended archaeol), which are believed to be mostly sourced by halophilic Euryarchaeota (Kates, 1977; Kamekura and Kates, 1999; Dawson et al., 2012; Lincoln et al., 2014a); these extremophiles live at high salt concentrations (up to 200 g/l; e.g., Oren, 2002). Cultures of halophilic archaea and mat or sediment samples from modern salt-rich environments dominated by halophilic euryarchaea are typified by the absence of GDGTs (e.g., Teixidor et al., 1993; Jahnke et al., 2008; Dawson et al., 2012). Caldarchaeol seems to be the only GDGT present in some ancient hypersaline depositional settings (Turich and Freeman, 2011; Birgel et al., 2014), but its source in these environments is unknown. The predominance of archaeol, as well as the presence of extended archaeol and caldarchaeol in the MSC sediments of the Pollenzo section, is consequently consistent with a hypersaline environment.

However, the overall archaeal lipid inventory also shows remarkable differences from other hypersaline settings. Unlike most modern and ancient hypersaline environments (cf. Teixidor et al., 1993; Turich and Freeman, 2011; Birgel et al., 2014), various GDGTs and not only caldarchaeol, archaeol, and extended archaeol are present in the Pollenzo section. In particular, crenarchaeol is among the most abundant GDGTs below and above the MSC onset. Crenarchaeol is known to be mainly produced by planktonic Thaumarchaeota (Schouten et al., 2013; Elling et al., 2017), typically autotrophs (Könneke et al., 2005) that live in the meso- to bathy-pelagic zones of modern oceans, where they account for up to 40% of all cells (Karner et al., 2001; Wuchter et al., 2006; Pearson and Ingalls, 2013). Thaumarchaeota are mostly found in seawater with normal salinity (~35 ppt), even though laboratory cultures of *Nitrosopumilus maritimus* suggest that salinities as high as 51 ppt may be tolerated without an effect on the GDGT distribution (Elling et al., 2015). However, it has been put forward that marine Euryarchaeota (Marine Group II) also produce crenarchaeol, but this hypothesis remains a matter of debate (Schouten et al., 2014; Lincoln et al., 2014a,b). Benthic ammonia-oxidizing archaea (Pitcher et al., 2011) may produce crenarchaeol as well. Molecular studies targeting various marine sediments revealed that an equal amount of caldarchaeol and crenarchaeol (caldarchaeol/crenarchaeol ratio ~1) is typical for a combined contribution from planktonic Thaumarchaeota and Euryarchaeota (e.g., Turich et al., 2007 and References therein), thus agreeing with normal marine conditions. Such a pattern has been reported from modern (e.g., Pearson and Ingalls, 2013) and Cenozoic marine sediments (Schouten et al., 2013), despite a more extended GDGT database (Kim et al., 2010) revealed that in modern open marine waters the caldarchaeol/crenarchaeol ratio can fluctuate between 0.5 and 1.5 (Fig. 5). The caldarchaeol/crenarchaeol ratio close to 1 of the pre-MSC Pollenzo deposits remains unchanged in the basal MSC deposits, where DGDs abruptly increase (e.g., Bed f), indicat-ing that marine planktonic Thaumarchaeota were still present during this early stage of the MSC. Yet, the sharp increase of the caldarchaeol/crenarchaeol ratio (up to 13) in the uppermost part of the section suggests a rapid decline of planktonic Thaumarchaeota in response to the establishment of harsher conditions in the water body, probably resulting from an intensification of water column stratification (see below).

5.2. Is the ACE index a reliable indicator of paleosalinity in Messinian strata?

The ACE index was introduced by Turich and Freeman (2011) as paleosalinity recorder in ancient sediments and has been applied with varying results and interpretations (e.g., Birgel et al., 2014; Günther et al., 2014; Huguet et al., 2015; Christeleit et al., 2015). For the Pollenzo section, the ACE index shows wide fluctuations across the MSC onset, although a general upward increase is observed in the carbonate layers (from 14 in Bed c to 67 in the Bed g), suggesting a rise in salinity (Fig. 3). However, the ACE salinity estimates obtained with the equation of Turich and Freeman (2011) (Eq. 3) are surprisingly high, not to say unrealistic for such evaporite-free sediments. The calculated salinities for pre-MSC waters range from 60 to 180 ppt. This is in great contrast with the micropaleontological content of the studied sediments (steno-haline planktonic and benthic foraminifers, calcareous nannofos-sils; Violanti et al., 2013), and the dominance of Thaumarchaeota suggested by the GDGT distribution, both indicative of normal marine salinities in the water column, similar to the present day Mediterranean Sea with its salinity of 36 ppt. The obtained ACE based salinities for the MSC waters as high as ~200 ppt (Bed g) fall within the range of gypsum precipitation (gypsum saturation point ~110 ppt; e.g., Natalicchio et al., 2014). However, no gypsum deposits have been observed at this level in the Pollenzo section, suggesting that the measured ACE salinities are flawed. In addition,
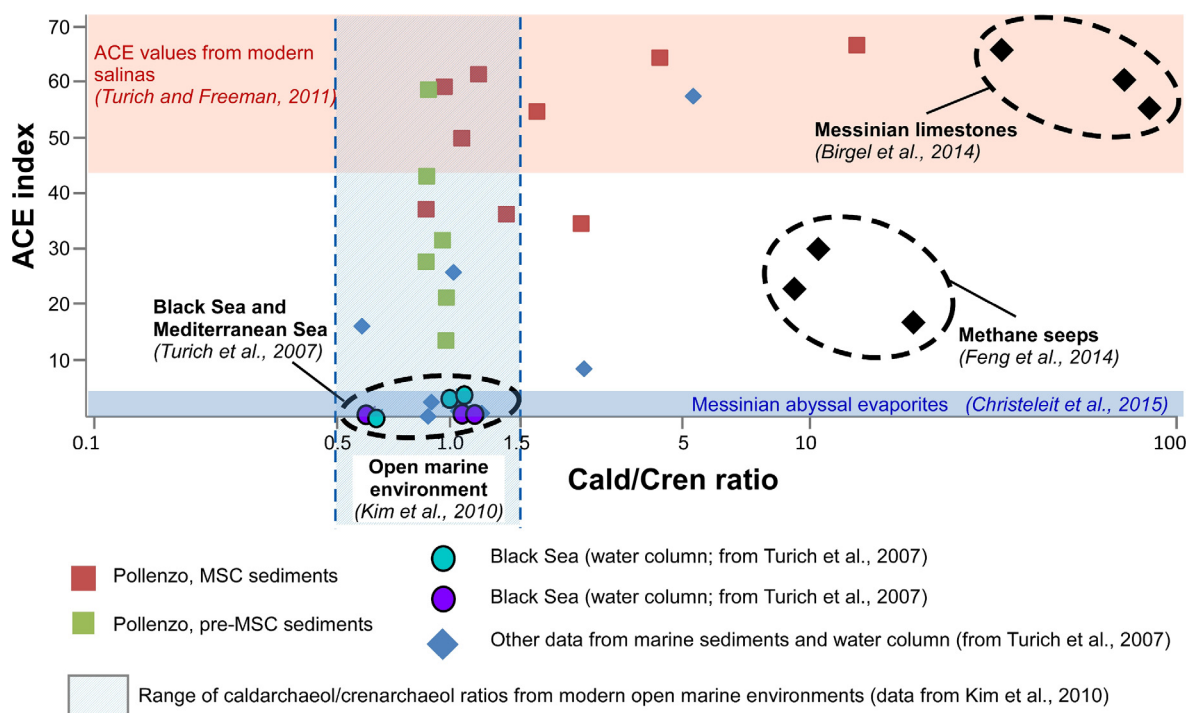

Fig. 5. Plot of the caldarchaeol/crenarchaeol (Cald/Cren) ratios against ACE index values for the Pollenzo samples. Samples from Messinian carbonates of Sicily and Calabria (Birgel et al., 2014), methane seeps (Feng et al., 2014) and other data from marine environments are included. The dashed shaded area indicates a global inventory of caldarchaeol/crenarchaeol ratios from modern oceans reported by Kim et al. (2010). The shaded blue and red areas represent ranges of ACE index values for Messinian abyssal deposits (Christeleit et al., 2015) and modern salinas (Turich and Freeman, 2011), respectively. (For interpretation of the references to colour in this figure legend, the reader is referred to the web version of this article.)

the negative $\delta^{18}O$ values (as low as $-9‰$ PDB) measured in MSC carbonate beds e, f and g (Dela Pierre et al., 2012) point to significant influx of freshwater during the early MSC, further questioning the reliability of ACE-based salinities in this case.

By comparison with other Mediterranean MSC sequences, inconsistencies between the estimated ACE paleosalinity and other independent salinity indicators (i.e. lithological features and the overall lipid biomarker inventory) are apparent. For example, Messinian evaporites (gypsum, anhydrite, and halite) studied by Christeleit et al. (2015) from the Mediterranean abyssal plain show ACE index values ranging from 0.3 to 3.1, which correspond to brackish to normal marine salinities. These values are surprisingly low considering that gypsum and halite precipitation requires salinities of ~110 and ~270 ppt (e.g., Natalicchio et al., 2014), respectively. Christeleit et al. (2015) hypothesized that the abyssal plain evaporites were deposited in deep stratified basins, typified by a mixed superficial water layer with normal salinity and a deep bottom water brine at or above the gypsum and halite saturation points. According to their scenario, the low ACE index values preserved in the evaporites record only the salinities of surface waters, which were dominated by planktonic Thaumarchaeota, the biomass of which was subsequently transported to the sediments. Even though lipid biomarkers from surface water communities can accumulate at the seafloor by an effective shuttle process (Taylor et al., 2013 and References therein), it must be stressed that the deep brines of modern stratified hypersaline basins, such as the deep Eastern Mediterranean Sea (van der Wielen et al., 2005) or the Dead Sea (Thomas et al., 2015) are inhabited by diverse microbial communities, also including halophilic archaea among other archaea and bacteria. Considering the modern analogs, it is difficult to imagine that the archaeal lipid inventory, and therefore the ACE index, of the abyssal plain evaporites studied by Christeleit et al. (2015) are not affected by these brine communities and only reflect the upper water column inventory of planktonic Thaumarchaeota. Assuming that the deep halophilic archaeal communities produce membrane lipids composed of DGDs, chiefly archaeol, the ACE index of the abyssal plain Messinian evaporites would be expected to be high. Only a few studies have reported high contents of DGDs (archaeol) from evaporitic deposits, including examples from Miocene halite of the Lorca Basin (Teixidor et al., 1993) and the Dead Sea (Oldenburg et al., 2000), but the GDGTs required to calculate the ACE index have not been measured. The only case in which ACE paleosalinity estimations agree with lithology and lipid inventory is represented by some MSC carbonates (the so called Calcare di Base) from Sicily and Calabria (Italy), where high ACE index values (> 40) reflecting salinities > 75 ppt were obtained (Turich and Freeman, 2011; Birgel et al., 2014). Additional indicators for increased salinities in these carbonates, including pseudomorphs after halite (Birgel et al., 2014; Caruso et al., 2015), the occurrence of extended archaeol, and characteristic GDGT patterns with almost only caldarchaeol present (Birgel et al., 2014), agree with high salinities and apparently reflect deposition in a hypersaline basin not typified by normal marine conditions and their characteristic dominance of planktonic Thaumarchaeota.

The inconsistency between the ACE salinity reconstruction and other proxies (e.g., lithology, fossil content) suggests that the ACE index should only be used with caution to calculate paleosalinities from Messinian strata with their different sources of archaeal lipids. Interestingly, studies of modern restricted environments with known salinities (Günther et al., 2014; Huguet et al., 2015) indicate that the ACE index is not necessarily dependent on salinity alone, but rather on the source of the archaeal lipids (archaeol and caldarchaeol) used for its calculation. Originally, the ACE index was calibrated using sediments and suspended particles from salt works (Turich and Freeman, 2011), where caldarchaeol is abundant and other GDGTs are only minor constituents or are even absent

(Turich et al., 2007). Therefore, it seems likely that the ACE index provides reliable salinity estimates only when caldarchaeol is the predominant GDGT like in some MSC carbonates (Calcare di Base) typified by caldarchaeol/crenarchaeol ratio $\gg 1.5$ (Fig. 5) and the presence of pseudomorphs after halite (Turich and Freeman, 2011; Birgel et al., 2014). It needs to be stressed that other sources of archaeal lipids, particularly sediment-dwelling archaea, will affect the calculation of the ACE index. Among benthic archaea, methanotrophic (Feng et al., 2014) and methanogenic (Koga et al., 1998; Schouten et al., 2013) Euryarchaeota produce large amounts of archaeol and caldarchaeol, which may also cause high caldarchaeol/crenarchaeol ratios and high ACE based salinity estimates (Fig. 5; Feng et al., 2014), which are, of course, not necessarily indicative of hypersaline conditions.

Based on these considerations, the calculation of ACE-based salinities can be biased by the production of ring-containing GDGTs by Thaumarchaeota and methanotrophic archaea. Since Thaumarchaeota produce both crenarchaeol and caldarchaeol (e.g., Schouten et al., 2013), the ACE index is unlikely to provide robust salinity estimates for marine settings that are characterized by thaumarchaeotal input to the caldarchaeol pool (caldarchaeol/crenarchaeol ratio ~1; e.g., Pearson and Ingalls, 2013). In this regard, we put forward that the caldarchaeol/crenarchaeol ratio must be monitored if the ACE index is to be used, to be able to decide whether the overall caldarchaeol pool is impacted by thaumarchaeotal caldarchaeol production or not (Fig. 5). Such a relationship applies to most of the Pollenzo samples that are characterized by a caldarchaeol/crenarchaeol ratio ~1; the high ACE index values (> 30) (Figs. 3 and 5) calculated from these sediments cannot be translated into realistic salinities. A different explanation is, however, needed for the few samples from the uppermost MSC deposits with high caldarchaeol/crenarchaeol ratios and ACE index values, which in turn result from high caldarchaeol and DGD (archaeol and extended archaeol) contents (see discussion below).

5.3. Do DGDs record the onset of hypersaline conditions in the Pollenzo section?

The DGD distribution in the uppermost Pollenzo section suggests an expansion of halophilic Euryarchaeota and an overall change in the archaeal community. Halophilic Euryarchaeota are generally thought to be aerobic heterotrophs, though alternative lifestyles including anaerobic and even phototrophic metabolisms have been suggested (Oren, 2002, 2014). Since the conditions in the water column of the Pollenzo section seem to have been locally still favorable for planktonic Thaumarchaeota even after the onset of the MSC, halophilic archaea may rather have lived at or below a chemocline, separating a body of normal marine or even brackish waters with oxic conditions above, from a layer of denser and more saline brines below. Interestingly, the major change and diversification in the archaeal lipid assemblage (just below Bed f) coincides with the appearance of the pentacyclic triterpenoid tetrahymanol. This compound has been attributed to bacterivorous ciliates (e.g., *Tetrahymena pyriformis*; Harvey and McManus, 1991), anoxygenic phototrophic bacteria (Kleemann et al., 1990; Rashby et al., 2007; Eickhoff et al., 2013), or aerobic methanotrophic bacteria (Banta et al., 2015), all of which are living at the interface between oxic and anoxic waters in stratified basins (Wakeham et al., 2007, 2012). Hence tetrahymanol is commonly used as an indicator of water column stratification (ten Haven et al., 1989; Schoell et al., 1994; Sinninghe Damsté et al., 1995). The appearance of this compound along with the evidence for a possible contemporaneous salinity increase points to the establishment of water column stratification in the Piedmont Basin.

However, the interpretation that the increase of DGDs and caldarchaeol had been caused by an increase of salinity and an associated change in the archaeal community is not without alternatives, particularly considering the lack of local lithological evidence for evaporation (see above). Some haloarchaea have been found to tolerate low salt concentrations for example at sulfur-rich springs (∼10 ppt; Elshahed et al., 2004) and in estuaries (Purdy et al., 2004). Similarly, Jessen et al. (2016) described several groups of extremophilic archaea and bacteria, including non-halophilic Thermoplasmatales and Halobacteriales in microbial mats on the seafloor of the Black Sea, which are dominated by filamentous *Beggiatoa*-like sulfide-oxidizing bacteria at a salinity of approximatively 20 ppt. These mats occur in hypoxic environments where the chemocline intercepts the seafloor. Since non-halophilic Thermoplasmatales are known to produce chiefly archaeol, extended archaeol, and caldarchaeol (de Rosa and Gambacorta, 1988; Schouten et al., 2013; Becker et al., 2016) and Halobacteriales produce mostly archaeol and extended archaeol (e.g., Dawson et al., 2012), these taxa are candidate source organisms that could explain the high DGD and caldarchaeol contents of the upper part of the Pollenzo section.

Remarkably, the sharp increase of these compounds in the sediments below Bed f of the Pollenzo section coincides with the first occurrence of filamentous fossils (Fig. 2D), which have been interpreted as sulfide-oxidizing bacteria (Dela Pierre et al., 2012, 2014). Moreover, high archaeal and bacterial cell densities and peaks of various molecular fossils, including GDGTs (especially caldarchaeol and crenarchaeol), archaeol and tetrahymanol, have also been reported from the chemocline of modern stratified basins, including the Black Sea (Wakeham et al., 2003, 2007) and the Cariaco Basin (Wakeham et al., 2012). Based on the striking similarities between the biomarker inventories of the Pollenzo sediments with those of some modern, non-evaporitic basins (Wakeham et al., 2003, 2007, 2012; Jessen et al., 2016), it seems possible that the Pollenzo section records the onset of the MSC in a marine basin that was typified by intense water column stratification and a well-defined chemocline, but not necessarily by desiccation and hypersaline conditions.

6. Conclusions

Archaeal molecular fossils, in particular isoprenoidal dialkyl glycerol diethers (DGDs) and isoprenoidal glycerol dialkyl glycerol tetraethers (GDGTs), are powerful tools for reconstructing environmental change in the course of the MSC in the absence of evaporites. The Piedmont Basin sedimentary rocks of the Pollenzo section record an increase and a diversification of Archaea approximately 20 ka after the advent of the crisis. The molecular fossils archived in the basal MSC sediments point to the existence of persistent marine to possibly brackish conditions in the upper water column. The increase of archaeol and caldarchaeol and the appearance of extended archaeol, mostly produced by extremophilic archaea (especially halophiles), after the onset of the MSC apparently suggest an increase of salinity. However, other evidence for hypersaline conditions is lacking except for the unrealistically high values of the Archaeol and Caldarchaeol Ecometric (ACE), representing salinities > 60 ppt for the entire section. The ACE index values obtained for the Pollenzo section cannot be translated into reliable salinities, since the archaeal lipid patterns are affected by shifts in the composition of archaeal communities that impede the utility of this proxy. We speculate that the changes in the archaeal community at the onset of the crisis do not necessarily account for basin-wide seawater evaporation, but may reflect stratification and hypoxia like in some modern stratified basins (Black Sea or the Cariaco Basin). Stratified, but not necessarily evaporitic basins may serve as a modern analog for a better understanding of the response of microorganisms to the MSC in some marginal basins of the Mediterranean Sea like the Piedmont Basin.

Appendix A. Supplementary material

Supplementary data associated with this article can be found, in the online version, at http://dx.doi.org/10.1016/j.orggeochem.2017.08.014. These data include Google maps of the most important areas described in this article.

Associate Editor—**Stefan Schouten**

References

Banta, A.B., Wie, J.H., Welander, P.V., 2015. A distinct pathway for tetrahymanol synthesis in bacteria. Proceedings of the National Academic of Sciences 112, 13478–13483.

Baudrand, M., Grossi, V., Pancost, R., Aloisi, G., 2010. Non-isoprenoid macrocyclic glycerol diethers associated with authigenic carbonates. Organic Geochemistry 61, 34–44.

Becker, K.W., Lipp, J.S., Zhu, C., Liu, X.-L., Hinrichs, K.-U., 2013. An improved method for the analysis of archaeal and bacterial ether core lipids. Organic Geochemistry 61, 34–44.

Becker, K.W., Elling, F.J., Yoshinaga, M.Y., Söllinger, A., Urich, T., Hinrichs, K.-U., 2016. Unusual butane- and pentanetriol-based tetraether lipids in *Methanomassiliicoccus luminyensis*, a representative of the seventh order of methanogens. Applied and Environmental Microbiology 82, 4505–4516.

Bellanca, A., Caruso, A., Ferruzza, G., Neri, R., Rouchy, J.M., Sprovieri, M., Blanc-Valleron, M.M., 2001. Transition from marine to hypersaline conditions in the Messinian Tripoli Formation from the marginal areas of the central Sicilian Basin. Sedimentary Geology 140, 87–105.

Birgel, D., Thiel, V., Hinrichs, K.-U., Elvert, M., Campbell, K.A., Reitner, J., Farmer, J.D., Peckmann, J., 2006. Lipid biomarker patterns of methane-seep microbialites from the Mesozoic convergent margin of California. Organic Geochemistry 37, 1289–1302.

Birgel, D., Himmler, T., Freiwald, A., Peckmann, J., 2008. A new constraint on the antiquity of anaerobic oxidation of methane: Late Pennsylvanian seep limestones from southern Namibia. Geology 36, 543–546.

Birgel, D., Guido, A., Liu, X., Hinrichs, K.-U., Gier, S., Peckmann, J., 2014. Hypersaline conditions during deposition of the Calcare di Base revealed from archaeal di- and tetraether inventories. Organic Geochemistry 77, 11–21.

Birgel, D., Meister, P., Lundberg, R., Horath, T.D., Bontognali, T.R.R., Bahniuk, A.M., De Rezende, C.E., Vasconcelos, C., McKenzie, J.A., 2015. Methanogenesis produces strong ^{13}C enrichment in stromatolites of Lagoa Salgada, Brazil: A modern analogue for Palaeo-/Neoproterozoic stromatolites? Geobiology 13, 245–266.

Blumenberg, M., Seifert, R., Reitner, J., Pape, T., Michaelis, W., 2004. Membrane lipid patterns typify distinct anaerobic methanotrophic consortia. Proceedings of the National Academy of Sciences 30, 11111–11116.

Blumenberg, M., Seifert, R., Petersen, S., Michaelis, W., 2007. Biosignatures present in a hydrothermal massive sulfide from the Mid-Atlantic Ridge. Geobiology 5, 435–450.

Capella, W., Matenco, L., Dmitrieva, E., Roest, W.M.J., Hessels, S., Hssain, M., Chakor-Alami, A., Sierro, F.J., Krijgsman, W., 2016. Thick-skinned tectonics closing the Rifian Corridor. Tectonophysics 710–711, 249–265.

Caruso, A., Pierre, C., Blanc-Valleron, M.-M., Rouchy, J.M., 2015. Carbonate deposition and diagenesis in evaporitic environments: The evaporative and sulphur-bearing limestones during the settlement of the Messinian Salinity Crisis in Sicily and Calabria. Palaeogeography, Palaeoclimatology, Palaeoecology 429, 136–162.

Christeleit, E.C., Brandon, M.T., Zhuang, G., 2015. Evidence for deep-water deposition of abyssal Mediterranean evaporites during the Messinian salinity crisis. Earth and Planetary Science Letters 427, 226–235.

Dawson, K.S., Freeman, K.H., Macalady, J.L., 2012. Molecular characterization of core lipids from halophilic archaea grown under different salinity conditions. Organic Geochemistry 48, 1–8.

De Rosa, M., Gambacorta, A., 1988. The lipids of archaebacteria. Progress in Lipid Research 27, 153–175.

Dela Pierre, F., Bernardi, E., Cavagna, S., Clari, P., Gennari, R., Irace, A., Lozar, F., Lugli, S., Manzi, V., Natalicchio, M., Roveri, M., Violanti, D., 2011. The record of the Messinian salinity crisis in the Tertiary Piedmont Basin (NW Italy): the Alba section revisited. Palaeogeography, Palaeoclimatology, Palaeoecology 310, 238–255.

Dela Pierre, F., Clari, P., Bernardi, E., Natalicchio, M., Costa, E., Cavagna, S., Lozar, F., Lugli, S., Manzi, V., Roveri, M., Violanti, D., 2012. Messinian carbonate-rich beds of the Tertiary Piedmont Basin (NW Italy): microbially-mediated products straddling the onset of the salinity crisis. Palaeogeography, Palaeoclimatology, Palaeoecology 344–345, 78–93.

Dela Pierre, F., Clari, P., Bernardi, E., Natalicchio, M., Ferrando, S., Giustetto, R., Lozar, F., Lugli, S., Manzi, V., Roveri, M., Violanti, D., 2014. Flocculent layers and bacterial mats in the mudstone interbeds of the Primary Lower Gypsum unit (Tertiary Piedmont basin, NW Italy): archives of palaeoenvironmental changes during the Messinian salinity crisis. Marine Geology 355, 71–87.

Dela Pierre, F., Natalicchio, M., Ferrando, S., Giustetto, R., Birgel, D., Carnevale, G., Gier, S., Lozar, F., Marabello, D., Peckmann, J., 2015. Are the large filamentous microfossils preserved in Messinian gypsum colorless sulfide-oxidizing bacteria? Geology 43, 855–858.

Eglinton, G., Hamilton, R.J., 1967. Leaf epicuticular waxes. Science 156, 1322–1335.

Eickhoff, M., Birgel, D., Talbot, H.M., Peckmann, J., Kappler, A., 2013. Oxidation of Fe (II) leads to increased C-2 methylation of pentacyclic triterpenoids in the anoxygenic phototrophic bacterium *Rhodopseudomonas palustris* strain TIE-1. Geobiology 11, 268–278.

Elling, F.J., Könneke, M., Mußmann, M., Greve, A., Hinrichs, K.-U., 2015. Influence of temperature, pH, and salinity on membrane lipid composition and TEX$_{86}$ of marine planktonic thaumarchaeal isolates. Geochimica et Cosmochimica Acta 171, 238–255.

Elling, F.J., Könneke, M., Nicol, G.W., Stiegelmeier, M., Bayer, B., Spieck, E., de la Torre, J.R., Becker, K.W., Thomm, M., Prosser, J.I., Herndl, G.J., Schleper, C., Hinrichs, K.-U., 2017. Chemotaxonomic characterisation of the thaumarchaeal lipidome. Environmental Microbiology 19, 2681–2700.

Elshahed, M.S., Najar, F.Z., Roe, B.A., Oren, A., Dewers, T.A., Krumholz, L.R., 2004. Survey of archaeal diversity reveals an abundance of halophilic archaea in a low-salt, sulfide- and sulfur-rich spring. Applied and Environmental Microbiology 70, 2230–2239.

Feng, D., Birgel, D., Peckmann, J., Roberts, H.H., Joye, S.B., Sassen, R., Liu, X.-L., Hinrichs, K.-U., Chen, D., 2014. Time integrated variation of sources of fluids and seepage dynamics archived in authigenic carbonates from Gulf of Mexico Gas Hydrate Seafloor Observatory. Chemical Geology 385, 129–139.

Flecker, R., Krijgsman, W., Capella, W., de Castro Martíns, C., Dmitrieva, E., Mayser, J. P., Marzocchi, A., Modestou, S., Ochoa, D., Simon, D., Tulbure, M., van den Berg, B., van der Schee, M., de Lange, G., Ellam, R., Govers, R., Gutjahr, M., Hilgen, F., Kouwenhoven, T., Lofi, J., Meijer, P., Sierro, F.J., Bachiri, N., Barhoun, N., Alami, A. C., Chacon, B., Flores, J.A., Gregory, J., Howard, J., Lunt, D., Ochoa, M., Pancost, R., Vincent, S., Yousfi, M.Z., 2015. Evolution of the Late Miocene Mediterranean-Atlantic gateways and their impact on regional and global environmental change. Earth-Science Reviews 150, 365–392.

Gennari, R., Manzi, V., Angeletti, L., Bertini, A., Biffi, U., Ceregato, A., Faranda, C., Gliozzi, E., Lugli, S., Menichetti, E., Rosso, A., Roveri, M., Taviani, M., 2013. A shallow water record of the onset of the Messinian salinity crisis in the Adriatic foredeep (Legnagnone section, Northern Apennines). Palaeogeography, Palaeoclimatology, Palaeoecology 386, 145–164.

Gennari, R., Lozar, F., Turco, E., Dela Pierre, F., Manzi, V., Natalicchio, M., Lugli, S., Roveri, M., Schreiber, B.C., Taviani, M., in press. Integrated stratigraphy and paleoceanographic evolution of the pre-evaporitic phase of the Messinian salinity crisis in the Eastern Mediterranean as recorded in the Tokhni section (Cyprus island). Newsletters on Stratigraphy. https://doi.org/10.1127/nos/2017/0350 (in press).

Grice, K., Schouten, S., Nissenbaum, A., Charrach, J., Sinninghe Damsté, J.S., 1998. Isotopically heavy carbon in the C$_{21}$ to C$_{25}$ regular isoprenoids in halite-rich deposits from the Sdom Formation, Dead Sea Basin, Israel. Organic Geochemistry 28, 349–359.

Günther, F., Thiele, A., Gleixner, G., Xu, B., Yao, T., Schouten, S., 2014. Distribution of bacterial and archaeal ether lipids in soils and surface sediments of Tibetan lakes: Implications for GDGT-based proxies in saline high mountain lakes. Organic Geochemistry 67, 19–30.

Harvey, H.R., McManus, G.B., 1991. Marine ciliates as a widespread source of tetrahymanol and hopan-3β-ol in sediments. Geochimica et Cosmochimica Acta 55, 3387–3390.

Hopmans, E.C., Weijers, J.W.H., Schefuß, E., Herfort, L., Sinninghe Damsté, J.S., Schouten, S., 2004. A novel proxy for terrestrial organic matter in sediments based on branched and isoprenoid tetraether lipids. Earth and Planetary Sciences Letters 224, 107–116.

Hsü, K., Montadert, L., Bernoulli, D., Cita, M.B., Erickson, A., Garrison, R.E., Kidd, R.B., Mèlierés, F., Müller, C., Wright, R., 1977. History of the Mediterranean salinity crisis. Nature 267, 399–403.

Huguet, A., Grossi, V., Belmahdi, I., Fosse, C., Derenne, S., 2015. Archaeal and bacterial tetraether lipids in tropical ponds with contrasting salinity (Guadeloupe, French West Indies): implications for tetraether-based environmental proxies. Organic Geochemistry 83–84, 158–169.

Jahnke, L.L., Orphan, V.J., Embaye, T., Turk, K.A., Kubo, M.D., Summons, R.E., Des Marais, D.J., 2008. Lipid biomarker and phylogenetic analyses to reveal archaeal biodiversity and distribution in hypersaline microbial mat and underlying sediment. Geobiology 6, 394–410.

Jessen, G.L., Lichtschlag, A., Struck, U., Boetius, A., Reese, B.K., Texas, A., Christi, M.U., 2016. Distribution and composition of thiotrophic mats in the hypoxic zone of the Black Sea (150–170 m water depth, Crimea margin). Frontiers in Microbiology 7, 1–14.

Kamekura, M., Kates, M., 1999. Structural diversity of membrane lipids in members of Halobacteriaceae. Bioscience, Biotechnology and Biochemistry 63, 969–972.

Karner, M.B., DeLong, E.F., Karl, D.M., 2001. Archaeal dominance in the mesopelagic zone of the Pacific Ocean. Nature 409, 507–510.

Kates, M., 1977. The phytanyl ether-linked polar lipids and isoprenoid neutral lipids of extremely halophilic bacteria. Progress in the Chemistry of Fats and other Lipids 15, 301–342.

Kim, J.-H., van der Meer, J., Schouten, S., Helmke, P., Willmott, V., Sangiorgi, F., Koç, N., Hopmans, E.C., Sinninghe Damsté, J.S., 2010. New indices and calibrations derived from the distribution of crenarchaeol isoprenoid tetraether lipids: implications for past sea surface temperature reconstruction. Geochimica et Cosmochimica Acta 74, 4639–4654.

Kleemann, G., Poralla, K., Englert, G., Kjosen, H., Liaaen-Jensen, S., Neunlist, S., Rohmer, M., 1990. Tetrahymanol from the phototrophic bacterium *Rhodopseudomonas palustris*: first report of a gammacerane triterpene from a prokaryote. Journal of General Microbiology 136, 2551–2553.

Koga, Y., Morii, H., Akagawa-Matsushita, M., Ohga, M., 1998. Correlation of polar lipid composition with 16S rRNA phylogeny in methanogens. Further analysis of lipid component parts. Bioscience, Biotechnology and Biochemistry 62, 230–236.

Könneke, M., Bernhard, A.E., de la Torre, J.R., Walker, C.B., Waterbury, J.B., Stahl, D.A., 2005. Isolation of an autotrophic ammonia-oxidizing marine archaeon. Nature 437, 543–546.

Krijgsman, W., Hilgen, F., Raffi, I., Sierro, F., Wilson, D., 1999. Chronology, causes and progression of the Messinian salinity crisis. Nature 400, 652–655.

Laskar, J., Robutel, P., Joutel, F., Gastineau, M., Correia, A.C.M., Levrard, B., 2004. A long-term numerical solution for the insolation quantities of the Earth. Astronomy and Astrophysics 428, 261–285.

Lincoln, S.A., Wai, B., Eppley, J.M., Church, M.J., Summons, R.E., DeLong, E.F., 2014a. Planktonic Euryarchaeota are a significant source of archaeal tetraether lipids in the ocean. Proceedings of the National Academic of Sciences USA 111, 9858–9863.

Lincoln, S.A., Wai, B., Eppley, J.M., Church, M.J., Summons, R.E., DeLong, E.F., 2014b. Reply to Schouten et al.: Marine Group II planktonic Euryarchaeota are significant contributors to tetraether lipids in the ocean. Proceedings of the National Academic of Sciences USA 111, E4286.

Liu, X.-L., Summons, R.E., Hinrichs, K.-U., 2012. Extending the known range of glycerol ether lipids in the environment: structural assignments based on tandem mass spectral fragmentation patterns. Rapid Communications in Mass Spectrometry 26, 2295–2302.

Lozar, F., Violanti, D., Dela Pierre, F., Bernardi, E., Cavagna, S., Clari, P., Irace, A., Martinetto, E., Trenkwalder, S., 2010. Calcareous nannofossils and foraminifers herald the Messinian Salinity Crisis: The Pollenzo section (Alba, Cuneo; NW Italy). Geobios 43, 21–32.

Lozar, F., Violanti, D., Bernardi, E., Dela Pierre, F., Natalicchio, M., 2017. Identifying the onset of the Messinian salinity crisis: a reassessment of the biochronostratigraphic tools (Piedmont Basin, NW Italy). Newsletter on Stratigraphy doi: http://dx.doi.org/10.1127/nos/2017/0354 (in press).

Maino, M., Decarlis, A., Felletti, F., Seno, S., 2013. Tectono-sedimentary evolution of the Tertiary Piedmont Basin (NW Italy) within the Oligo-Miocene central Mediterranean geodynamics. Tectonics 32, 593–619.

Manzi, V., Roveri, M., Gennari, R., Bertini, A., Biffi, U., Giunta, S., Maria, S., Lanci, L., Lugli, S., Negri, A., Riva, A., Edoardo, M., Taviani, M., 2007. The deep-water counterpart of the Messinian Lower Evaporites in the Apennine foredeep: The Fanantello section (Northern Apennines, Italy). Palaeogeography, Palaeoclimatology, Palaeoecology 251, 470–499.

Manzi, V., Gennari, R., Lugli, S., Roveri, M., Scafetta, N., Schreiber, B.C., 2012. High-frequency cyclicity in the Mediterranean Messinian evaporites: evidence for solar-lunar climate forcing. Journal of Sedimentary Research 82, 991–1005.

Manzi, V., Lugli, S., Roveri, M., Dela Pierre, F., Gennari, R., Lozar, F., Natalicchio, M., Schreiber, B.C., Taviani, M., Turco, E., 2016. The Messinian salinity crisis in Cyprus: a further step towards a new stratigraphic framework for Eastern Mediterranean. Basin Research 28, 207–236.

Natalicchio, M., Dela Pierre, F., Lugli, S., Lowenstein, T.K., Feiner, S.J., Ferrando, S., Manzi, V., Roveri, M., Clari, P., 2014. Did late Miocene (Messinian) gypsum precipitate from evaporated marine brines? Insights from the Piedmont Basin (Italy). Geology 42, 179–182.

Oldenburg, T.B.P., Rullkötter, J., Böttcher, M.E., Nissenbaum, A., 2000. Molecular and isotopic characterization of organic matter in recent and sub-recent sediments from the Dead Sea. Organic Geochemistry 31, 251–265.

Oren, A., 2002. Diversity of halophilic microorganisms: environments, phylogeny, physiology, and applications. Journal Microbiology & Biotechnology 28, 56–63.

Oren, A., 2014. Halophilic archaea on Earth and in space: growth and survival under extreme conditions. Philosophical Transactions of the Royal Society Mathematical, Physical and Engineering Sciences 372. https://doi.org/10.1098/rsta.2014.0194.

Pancost, R.D., Sinninghe Damsté, J.S., 2003. Carbon isotopic compositions of prokaryotic lipids as tracers of carbon cycling in diverse settings. Chemical Geology 195, 29–58.

Pearson, A., Ingalls, A.E., 2013. Assessing the use of archaeal lipids as marine environmental proxies. Annual Review of Earth and Planetary Sciences 41, 359–384.

Pester, M., Schleper, C., Wagner, M., 2011. The Thaumarchaeota: an emerging view of their phylogeny and ecophysiology. Current Opinion in Microbiology 14, 300–306.

Pitcher, A., Wuchter, C., Siedenberg, K., Schouten, S., Sinninghe Damsté, J.S., 2011. Crenarchaeol tracks winter blooms of ammonia-oxidizing Thaumarchaeota in the coastal North Sea. Limnology and Oceanography 56, 2308–2318.

Purdy, K.J., Cresswell-Maynard, T.D., Nedwell, D.B., McGenity, T.J., Grant, W.D., Timmis, K.N., Embley, T.M., 2004. Isolation of haloarchaea that grow at low salinities. Environmental Microbiology 6, 591–595.

Rashby, S.E., Sessions, A.L., Summons, R.E., Newman, D.K., 2007. Biosynthesis of 2-methylbacteriohopanepolyols by an anoxygenic phototroph. Proceedings of the National Academic of Sciences USA 104, 15099–15104.

Roveri, M., Lugli, S., Manzi, V., Schreiber, B.C., 2008. The Messinian Sicilian stratigraphy revisited: new insights for the Messinian salinity crisis. Terra Nova 20, 483–488.

Roveri, M., Flecker, R., Krijgsman, W., Lofi, J., Lugli, S., Manzi, V., Sierro, F.J., Bertini, A., Camerlenghi, A., De Lange, G., Govers, R., Hilgen, F.J., Hübscher, C., Meijer, P. T., Stoica, M., 2014. The Messinian Salinity Crisis: Past and future of a great challenge for marine sciences. Marine Geology 352, 25–58.

Ryan, W.B.F., 2009. Decoding the Mediterranean salinity crisis. Sedimentology 56, 95–136.

Schoell, M., Hwang, R.J., Carlson, R.M.K., Welton, J.E., 1994. Carbon isotopic composition of individual biomarkers in gilsonites (Utah). Organic Geochemistry 21, 673–683.

Schouten, S., Hopmans, E.C., Forster, A., van Breugel, Y., Kuypers, M.M.M., Sinninghe Damsté, J.S., 2003. Extremely high sea-surface temperatures at low latitudes during the middle Cretaceous as revealed by archaeal membrane lipids. Geology 31, 1069–1072.

Schouten, S., Forster, A., Panoto, F.E., Sinninghe Damsté, J.S., 2007. Towards calibration of the TEX$_{86}$ palaeothermometer for tropical sea surface temperatures in ancient greenhouse worlds. Organic Geochemistry 38, 1537–1546.

Schouten, S., Hopmans, E.C., Sinninghe Damsté, J.S., 2013. The organic geochemistry of glycerol dialkyl glycerol tetraether lipids: a review. Organic Geochemistry 54, 19–61.

Schouten, S., Villanueva, L., Hopmans, E.C., van der Meer, M.T.J., Sinninghe Damsté, J. S., 2014. Are Marine Group II Euryarchaeota significant contributors to tetraether lipids in the ocean? Proceedings of the National Academic of Sciences USA 111, E4285.

Sierro, F.J., Hilgen, F.J., Krijgsman, W., Flores, J.A., 2001. The Abad composite (SE Spain): a Mediterranean and global reference section for the Messinian. Palaeogeography, Palaeoclimatology, Palaeoecology 168, 141–169.

Sinninghe Damsté, J.S., Kenig, F., Koopmans, M.P., Köster, J., Schouten, S., Hayes, J.M., de Leeuw, J.W., 1995. Evidence for gammacerane as an indicator of water column stratification. Geochimica et Cosmochimica Acta 59, 1895–1900.

Taylor, K.W., Huber, M., Hollis, C.J., Hernandez-Sanchez, M.T., Pancost, R.D., 2013. Re-evaluating modern and Palaeogene GDGT distributions: Implications for SST reconstructions. Global and Planetary Change 108, 158–174.

Teixidor, P., Grimalt, J.O., Pueyo, J.J., Rodriguez-Valer, F., 1993. Isopranylglycerol di-ethers in non-alkaline evaporitic environments. Geochimica et Cosmochimica Acta 57, 4479–4489.

ten Haven, H.L., Rohmer, M., Rullkötter, J., Bisseret, P., 1989. Tetrahymanol, the most likely precursor of gammacerane, occurs ubiquitously in marine sediments. Geochimica et Cosmochimica Acta 53, 3073–3079.

Thomas, C., Ionescu, D., Ariztegui, D., Scientific Team, D.S.D.D.P., 2015. Impact of paleoclimate on the distribution of microbial communities in the subsurface sediment of the Dead Sea. Geobiology 13, 546–561.

Turich, C., Freeman, K.H., 2011. Archaeal lipids record paleosalinity in hypersaline systems. Organic Geochemistry 42, 1147–1157.

Turich, C., Freeman, K.H., Bruns, M.A., Conte, M., Jones, A.D., Wakeham, S.G., 2007. Lipids of marine Archaea: Patterns and provenance in the water-column and sediments. Geochimica et Cosmochimica Acta 71, 3272–3291.

van der Wielen, P.W., Bolhuis, H., Borin, S., Daffonchio, D., Corselli, C., Giuliano, L., D'Auria, G., de Lange, G.J., Huebner, A., Varnavas, S.P., Thomson, J., Tamburini, C., Marty, D., McGenity, T.J., Timmis, K.N., Party, BioDeep Scientific, 2005. The enigma of prokaryotic life in deep hypersaline anoxic basins. Science 307, 121–123.

Violanti, D., Lozar, F., Natalicchio, M., Dela Pierre, F., Bernardi, E., Clari, P., Cavagna, S., 2013. Stress-tolerant microfossils of a Messinian succession from the Northern Mediterranean basin (Pollenzo section, Piedmont, northwestern Italy). Bollettino della Società Paleontologica Italiana 52, 45–54.

Wakeham, S.G., Lewis, C.M., Hopmans, E.C., Schouten, S., Sinninghe Damsté, J.S., 2003. Archaea mediate anaerobic oxidation of methane in deep euxinic waters of the Black Sea. Geochimica et Cosmochimica Acta 67, 1359–1374.

Wakeham, S.G., Amann, R., Freeman, K.H., Hopmans, E.C., Jørgensen, B.B., Putnam, I. F., Schouten, S., Sinninghe Damsté, J.S., Talbot, H.M., Woebken, D., 2007. Microbial ecology of the stratified water column of the Black Sea as revealed by a comprehensive biomarker study. Organic Geochemistry 38, 2070–2097.

Wakeham, S.G., Turich, C., Schubotz, F., Podlaska, A., Li, X.N., Varela, R., Astor, Y., Sáenz, J.P., Rush, D., Sinninghe Damsté, J.S., Summons, R.E., Scranton, M.I., Taylor, G.T., Hinrichs, K.-U., 2012. Biomarkers, chemistry and microbiology show chemoautotrophy in a multilayer chemocline in the Cariaco Basin. Deep-Sea Research I 63, 133–156.

Wang, H., Liu, W., Zhang, C.L., Jiang, H., Dong, H., Lu, H., Wang, J., 2013. Assessing the ratio of archaeol to caldarchaeol as a salinity proxy in highland lakes on the northeastern Qinghai-Tibetan Plateau. Organic Geochemistry 54, 69–77.

Wuchter, C., Abbas, B., Coolen, M.J.L., Herfort, L., van Bleijswijk, J., Timmers, P., Strous, M., Teira, E., Herndl, G.J., Middelburg, J.J., Schouten, S., Sinninghe Damsté, J.S., 2006. Archaeal nitrification in the ocean. Proceedings of the National Academic of Sciences USA 103, 12317–12322.